Erosive Wear and Corrosion in Hydrogenated and Silicon DLC Film Deposited on Carbon Steel

A. H. S. Bueno[a,c] 🔘 , J. Solis[b,c], H. Zhao[c], C. Wang[c], T. A. Simões[a,d,e] 🔘 , C. E. V. Masalla[a] 🔘 ,

A. Malacarne[a], R. C. Souza[a*] 🔘 , R. M. D. Brydson[d], R. Barker[c], A. Neville[c]

[a]*Universidade Federal de São João del-Rei, Praça Frei Orlando, 170, 36307-352, São João del-Rei, MG, Brasil.*
[b]*Instituto Tecnológico de Tlalnepantla, 54070, Tlalnepantla, México.*
[c]*University of Leeds, Institute of Functional Surfaces, Woodhouse Lane, LS2 9JT, Leeds, England.*
[d]*University of Leeds, School of Chemical and Process Engineering, LS2 9JT, Leeds, England.*
[e]*Universidade Federal do Recôncavo da Bahia, Centro de Ciência e Tecnologia em Energia e Sustentabilidade, 44085-132, Feira de Santana, BA, Brasil.*

Amongst numerous traditional coatings to protect internal surfaces, Diamond-Like Carbon (DLC) films attract significant interest from many industries, due to the ability of these coatings to overcome the toxic and/or environmentally unfriendly aspects of some common deposition techniques, especially electroplating. In addition, DLC coatings can be used to reduce corrosion, wear and importantly, abrasion on the inside of components, providing improved efficiency and prolonged lifetime. This work evaluates the performance of hydrogenated and silicon DLC coatings deposited by Plasma-Enhanced Chemical Vapour Deposition (PECVD) on carbon steel in terms of their erosion and electrochemical corrosion resistance. Erosion studies were conducted in a saline solution under different velocities and sand concentrations - modelling the direct impingement of high velocity, sand-laden fluid encountered in multiphase equipment flow. These experiments showed that for all impingement velocities, the Si-DLC exhibited lower mass loss. This coating enhanced integrity against erosion-corrosion acting together under saline environments with sand. The enhanced resistance was attributed to improved ductility of the surface layer, as well as the generation of an effective corrosion barrier which reduced pitting corrosion and suppressed significantly the anodic reaction.

Keywords: *Carbon-based Coatings, PECVD Coatings, Jet Impingement, Carbon Steel, Erosion, Corrosion.*

1. Introduction

Erosion-corrosion processes are one of the most common and costly mechanisms of damage caused in equipment that has fluid transportation. Erosion-corrosion is a tribo-corrosion process, where the material loss mechanism can be influenced by both mechanical and electrochemical processes. For the specific case of multiphase fluids it is associated to the metal loss on the internal surface; on one hand, the electrochemical dissolution associated with the aggressive environmental oil and slurry sand, which contains water, oxygen and ions such as chloride and sulphate. On the other hand, the mechanical erosion caused by fluid velocities and sand particles promotes impingement on the internal surface of equipment. Often, a major aspect of damage occurs from the interaction between erosion and corrosion, that triggers the process of erosion-corrosion and can be responsible for enhanced damage inside equipment[1-5].

Selection of new materials to be used under conditions of erosion-corrosion becomes central to the evasion of damage by material degradation of these components.

Several researchers have developed empirical models in order to understand the interactions of certain parameters and environmental conditions that affect the material loss as to improve materials selection. Some of the studied parameters and their corresponding conditions can be described as follows: fluid (composition, temperature, flow velocities, pressure of CO_2 gas, wettability of the fluid, fluid density, types of crude oil and inhibitors), solid particles (sand content, size, attack angle of the particles, hardness, density and velocity) and steel (type, hardness, microstructure, strength, ductility and toughness)[3-11]. However, the API-RP-14E standard used for industries to enable the determination of conditions for critical erosion velocities does not consider any of these apart from fluid density[12].

To increase the erosion and corrosion resistance on metallic materials exposed to aggressive environments, research has focused on use of advanced surface engineering technologies, in particular, DLC coatings[5,6,13]. According to the literature[1,2,11,14-16], the inherent properties of these protective materials, such as highly stable amorphous structure, hydrophobicity, high corrosion resistance, high thermal conductivity, high electrical

resistivity, high Young`s modulus, high hardness, wear and abrasion resistance[14,15,17-21] make them suitable candidates to assist in managing the detrimental effects of erosion-corrosion. In addition, given that DLC coatings commonly possess a low coefficient of friction, the efficiency in transport of fluids could be enhanced[13,22,23]. The erosion resistance of DLC films is linked to their elastic modulus, hardness, fracture toughness and the impact angle of the sand particles. Failure of DLC coatings starts with material loss caused by the abrasion impact of sand particles and corresponding initiation of dominant cracks. These cracks can grow and propagate, interact (crack coalescence) and eventually cause delamination of the coating. According to some authors, this mechanism of failure is known as "erosive fatigue wear"[5,8,24,25].

In our previous work[24,26,27], we have shown the susceptibility of DLC films (H or Si) to tribocorrosion. The present work aims to understand the influence of flow velocity and sand concentration on the erosion and corrosion resistance of hydrogenated DLC and hydrogenated-silicon DLC coatings deposited on carbon steel.

2. Materials and Methods

2.1. Materials

In this work, API X65 carbon steel was used as a substrate for H-DLC and Si-DLC coatings. Samples were produced in a disc shape with $\varnothing$ 25 mm x 6 mm thick, that were mechanically polished with 1 μm diamond suspension (Ra = 0.08 μm), followed by cleaning in ultrasonic acetone bath for 10 min. Then, the substrates were rinsed in deionised water and dried using compressed air. Before any deposition, they were cleaned inside the chamber using argon ion sputtering.

Both films (H-DLC and Si-DLC) were produced by PECVD technique with C_2H_2 gas at 0.3 Pa pressure as reaction gas. Acetylene was selected based on its accessibility, cost-effectiveness, and established performance in previous studies for the deposition of protective films. The pulsed bias was 780 V with a frequency of 40 kHz for plasma.

The initial deposition steps were identical for both films. The substrates were maintained at a temperature below 200 °C, and an adherent Cr interlayer was first applied using DC magnetron sputtering. Subsequently, the DLC coatings were deposited: Cr/WC/a-C:H with a hydrogen content of 20–40% at. for H-DLC at a deposition rate of 0.8 μm/min, and Si-a-C:H for Si-DLC at a deposition rate of 0.6 μm/min.

2.2. Characterization of the DLC coatings

A two-dimensional contact profilometer (Talysurf 5, Taylor-Hobson, UK) was used to evaluate the surface roughness. Data of 8 mm traces were analysed to the least square line, with a Gaussian filter, 0.25 mm upper cut-off and bandwidth 100 ± 1.

A diamond nano-indenter (Berkovich tip) with depth-sensing was used to evaluate hardness and elastic modulus. The nano-indentation was carried out at Micro Materials, Wrexham UK, in an enclosed box platform with regulated temperature, software suite and micro capture camera. A 1 to 100 mN depth-incremental load was used with a matrix of 50 indents. The criteria used to prevent substrate effects was a maximum penetration of 10% of the film thickness.

The thickness of the coating was determined by the abrasion ball cratering technique utilizing a calotester apparatus (Tribotechnic, France).

Atomic Force Microscopy (AFM, Bruker, ICON dimension with scan assist) was used to analyse the surface topography. The surfaces were cleaned with acetone before analysis. A total area of 100 μm² was scanned using a silicon tip (cantilever stiffness 0.4 N/m and tip radius of 10 nm) in contact mode to provide morphology samples data.

The multilayers (substrate, adhesion and DLC layers) were analysed by field emission scanning electron microscopy (SEM) using a Zeiss EVO MA15 Variable Pressure SEM with a coupled Energy-dispersive X-ray (EDX) spectrometer operated at 20 kV.

2.3. Jet impingement

The re-circulating jet impingement system that simulated the erosion process for the DLC coatings uses a centrifugal pump to mix the solution with sand particles (Figure 1) and then, the combined fluid is propelled through a dual nozzle system (4 mm bore diameter) with an incidence (impact) angle of 90⁰. The specimens had a 5 mm stand-off distance from the nozzle in all tested conditions. The area of the specimens exposed to
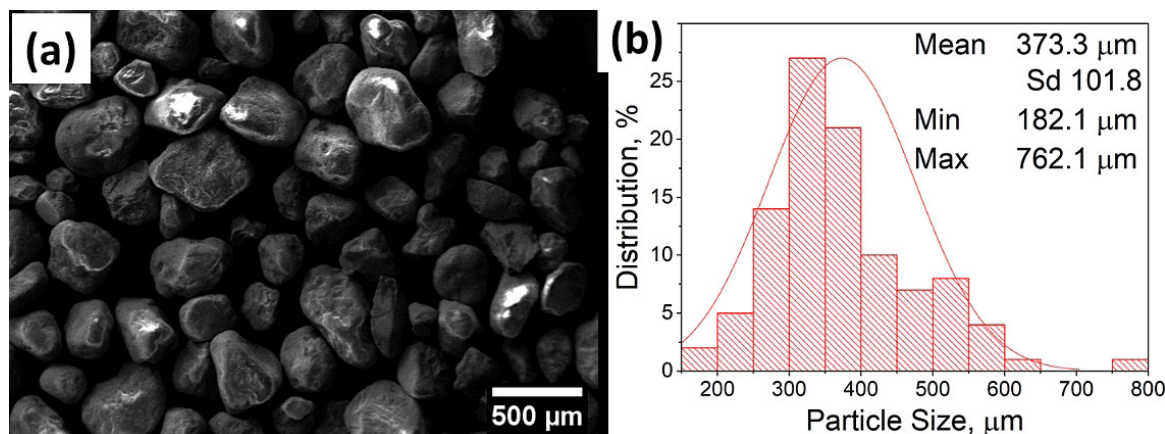

Figure 1. Sand particles used for erosion tests: (a) secondary electron image and (b) particle size distribution.

the slurry jet was 4.9 cm^2. All tests and measurements were repeated 3 times, and the average of results is reported in this work. The fluid used to simulate an erosive environment was a 3.5 wt% NaCl solution containing sand particles. The specimens were weighed before and after the tests to determine the total mass loss, using a balance with an accuracy of 0.001 mg. The surfaces analysis of the specimens were carried out by scanning electron microscopy (SEM) at the end of the test. The shown conditions in Table 1 were constant for each of the tests.

2.4. Electrochemical tests

A conventional three-electrode cell was used with platinum as a counter electrode, an Ag/AgCl reference electrode and the DLC film sample as a working electrode. A computer controlled potentiostat (Solartron potentiostat/galvanostat) was used for the electrochemical tests. Anodic polarization curves were acquired at a scan rate of 0.5 mV/s from -1.8 V to +0.5 V with respect to Open Circuit Potential (OCP). Electrochemical Impedance Spectroscopy (EIS) was setup with 5 mV (vs Ag/AgCl) amplitude and 30 kHz–10 mHz frequency range. The polarization and impedance tests were carried out with a solution of 3.5 wt% NaCl, at pH 6.5 and room temperature. Before starting the tests, samples were immersed in the solution for 30 min to stabilize the OCP.

3. Results and Discussion

3.1. Characterization prior to the erosion and electrochemical tests.

The elastic modulus and hardness of the H-DLC film were 181.2 ± 7 and 20.4 ± 3 GPa, respectively, while for

Table 1. Experimental conditions for erosion tests.

Duration of test	6 h
Fluid velocities	10 and 20 m/s
Temperature	20 °C
Incidence angle	90^0
Sand content	0, 5, 25, 132 and 187 mg/l

the Si-DLC film they were 132.6 ± 9 and 14.1 ± 4 GPa, respectively. The mechanical properties were in line with those previously observed by other authors[9,10,14,19,20]. Figure 2 shows the cratering created by the calotest. Coating thicknesses were determined to be 2.7 ± 0.2 μm and 1.6 ± 0.1 μm for the H-DLC and Si-DLC films, respectively.

Surface topography was analysed with AFM. Both DLC films showed compact and homogeneous characteristics and exhibited larger and smaller regions of height difference. The H-DLC film (Figure 3a) showed a surface with an average roughness (R$_a$) of 51 nm calculated from an area of 10 x 10 μm^2, while the Si-DLC (Figure 3b) had an R$_a$ of 97 nm. Both films showed an ordered array of nanoscale defects, being more pronounced for the Si-DLC coating than for H-DLC, which is confirmed by the roughness measurements.

According to Liu and Kwek[14], the formation of sp^3 bonds occurs when the DLC film surface receives carbon ions with a higher kinetic energy, which can be achieved by increasing the pulse bias during the deposition process. However, applying a pulse bias above 500V promotes formation of graphitic clusters in the DLC coating which causes surface roughness[14]. Since the DLC films were deposited at 780 V, it is expected a high concentration of graphitic-like species and the high roughness as observed by AFM, Figures 3a and 3b.

SEM was used to measure elemental thickness of the adhesion layers of Cr/WC for the H-DLC film and Cr/WSi for the Si-DLC film. Figure 4 and Figure 5 show SEM images, EDX maps and linescans of the DLC coating cross-sections, that show both the substrate/coating interface and a microdefect-free coating. The thicknesses of the H-DLC film, the chromium and tungsten adhesion interlayers were 2.8, 2.0 and 1.5 μm, respectively, on an iron-containing substrate. The WC interlayer forms a non-stoichiometric hydrogenated tungsten carbide WC:H, also known as W-C:H or W-DLC[26,27]. The Si-DLC film is composed of a 3.1 μm thick Si-DLC layer together chromium and tungsten adhesion layers both of thickness 2.2 μm.

3.2 Jet impingement

The erosion behavior of both DLC films under flux velocities of 10 and 20 m/s at different sand concentrations
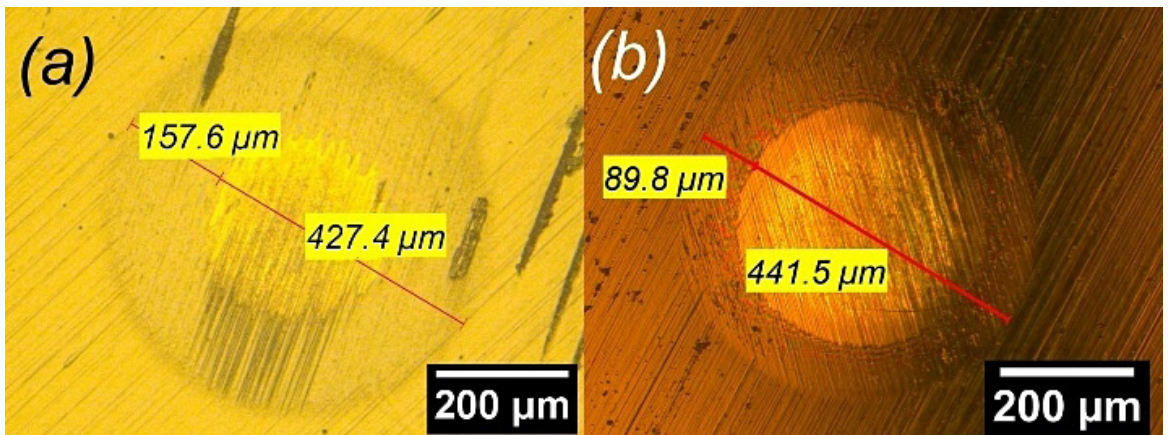

Figure 2. Craters from calotest of: (a) the H-DLC and (b) Si-DLC coatings.
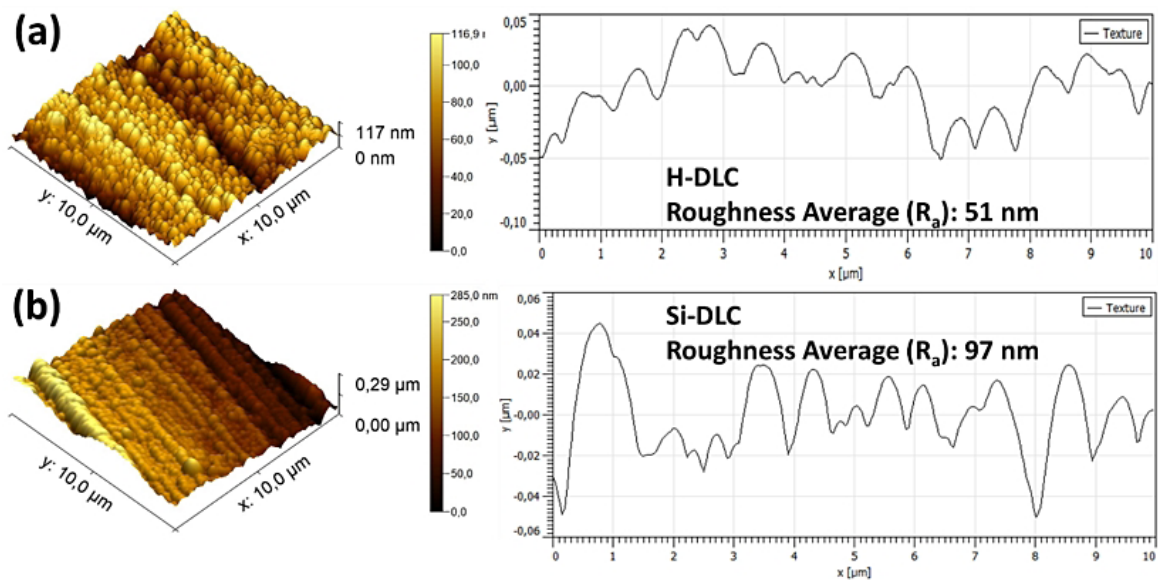
Figure 3. AFM images of the as deposited coatings: (a) H-DLC film and (b) Si-DLC.
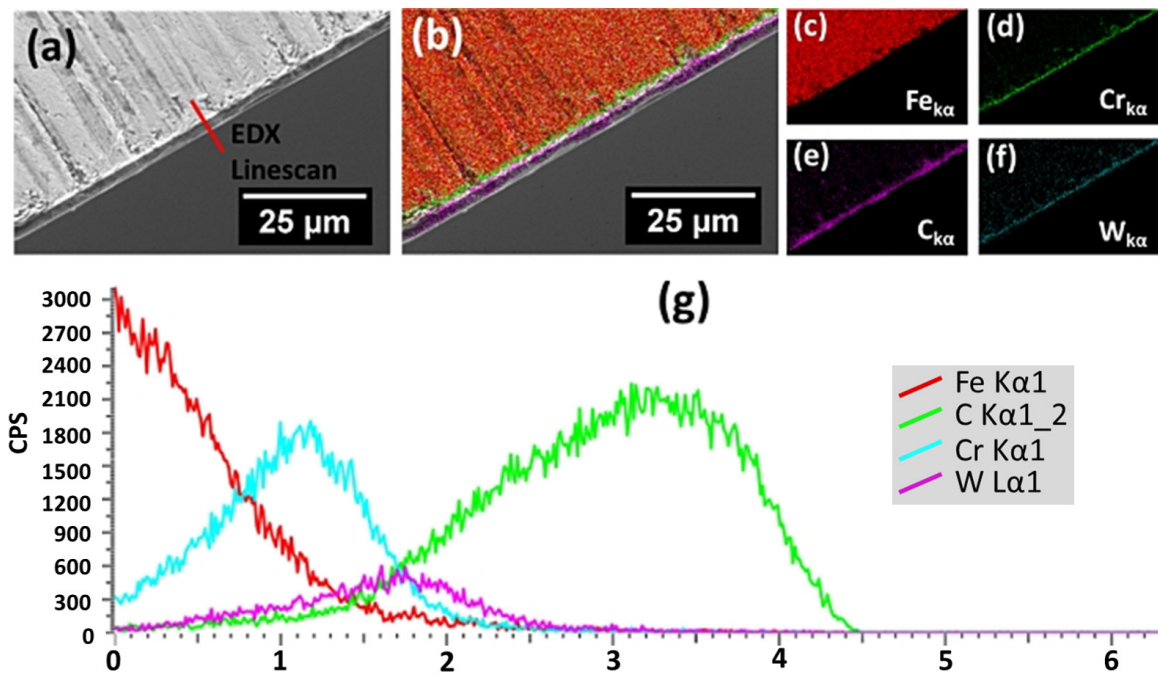

Figure 4. SEM analysis of H-DLC coating: (a) backscattered image, (b) composite EDX maps, (c-f) individual EDX maps for (c) Fe, (d) Cr, (e) C, (f) W and (g) EDX linescan cross section of the coating and substrate.

is depicted in Figure 6. For a velocity of 10 m/s without sand, both DLC coatings did not exhibit any measurable mass loss. Meanwhile, for sand concentrations of 5 mg/l, 25 mg/l, and 132 mg/l, a slightly increased mass loss was observed following each concentration increase. For a velocity of 20 m/s without sand, both DLC coatings presented low mass loss. However, increasing the sand concentration, the mass loss increases to values 4 times higher than those for a velocity of 10 m/s. For both particle flux velocities, the Si-DLC film underwent lower mass loss than the H-DLC film. Overall, the films had less mass loss when submitted to particle fluxes with low speed and concentration.

Figure 7 shows SEM secondary electron images of the DLC surfaces after erosion tests with a velocity of 10 m/s
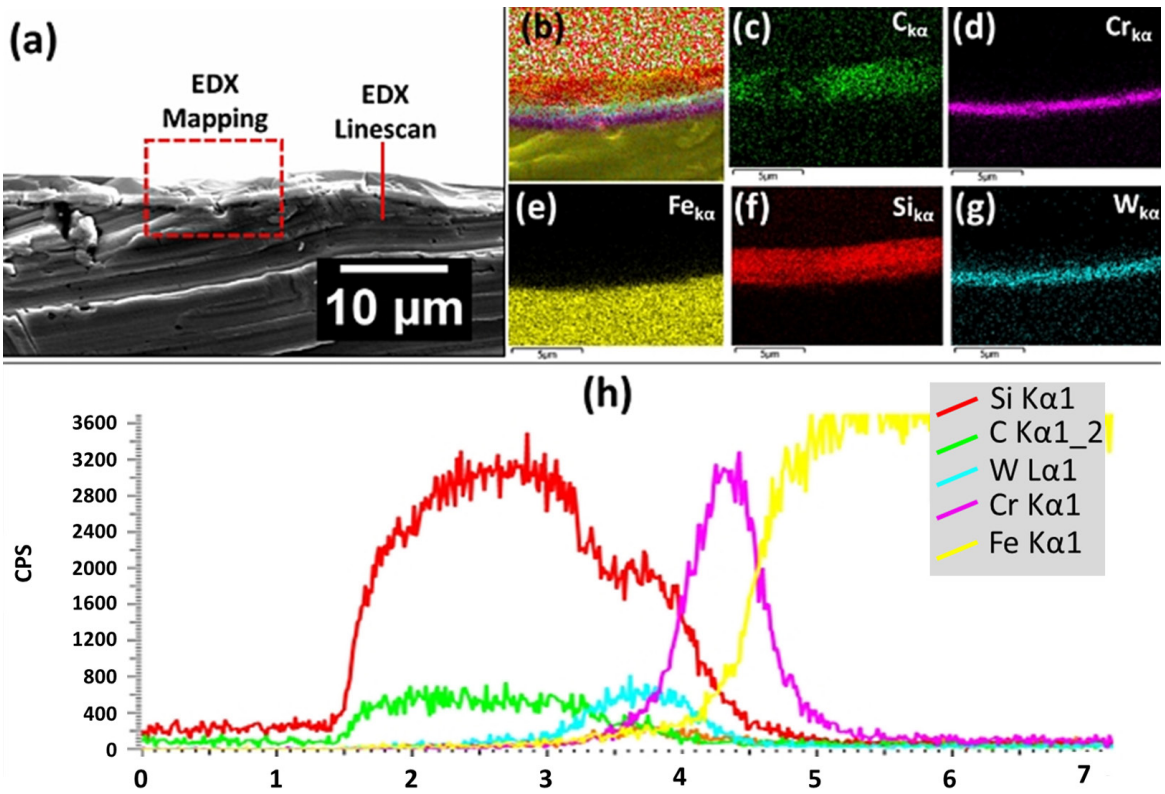
Figure 5. SEM analysis of Si-DLC coating: (a) backscattered image, (b) composite EDX maps, (c-g) individual EDX maps for (c) C, (d) Cr, (e) Fe, (f) Si, (g) W and (h) EDX linescan cross section of the coating and substrate.
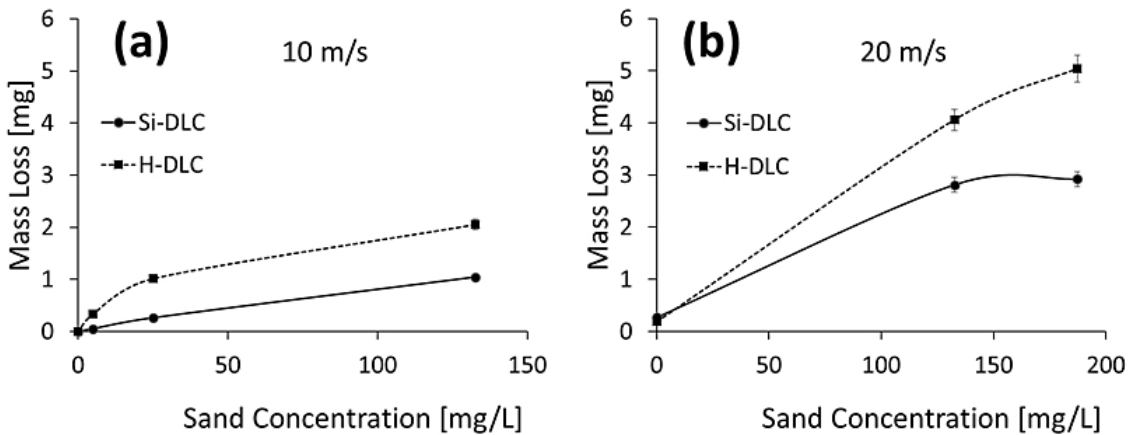

Figure 6. Erosion trends – mass loss vs. sand concentration for H-DLC and Si-DLC films at: (a) 10 m/s and (b) 20 m/s.

and for different sand concentrations. As expected, failure of the DLC coatings occurred sooner as the sand concentration increased. 5 mg/l of the impinging sand particles promoted the incidence of micro detachment in the DLC surfaces, being more severe in the H-DLC (see Figure 7a). For a 25 mg/l sand concentration, significantly larger and more areas of failure were visible on the surface of the DLC films (Figure 7b). When the sand concentration was increased to

132 mg/l, full removal of the coating occurred (Figure 7c). Progressive erosive loading promotes interaction between cracks causing micro detachment processes on the DLC surface and the final coating removal with the consequent exposure of the metal substrate to the corrosive solution[5].

Jellesen et al.[6] have suggested that when a thin DLC coating is in contact with soft metallic materials, such as carbon steel or stainless steel, and is subjected to erosive conditions, its
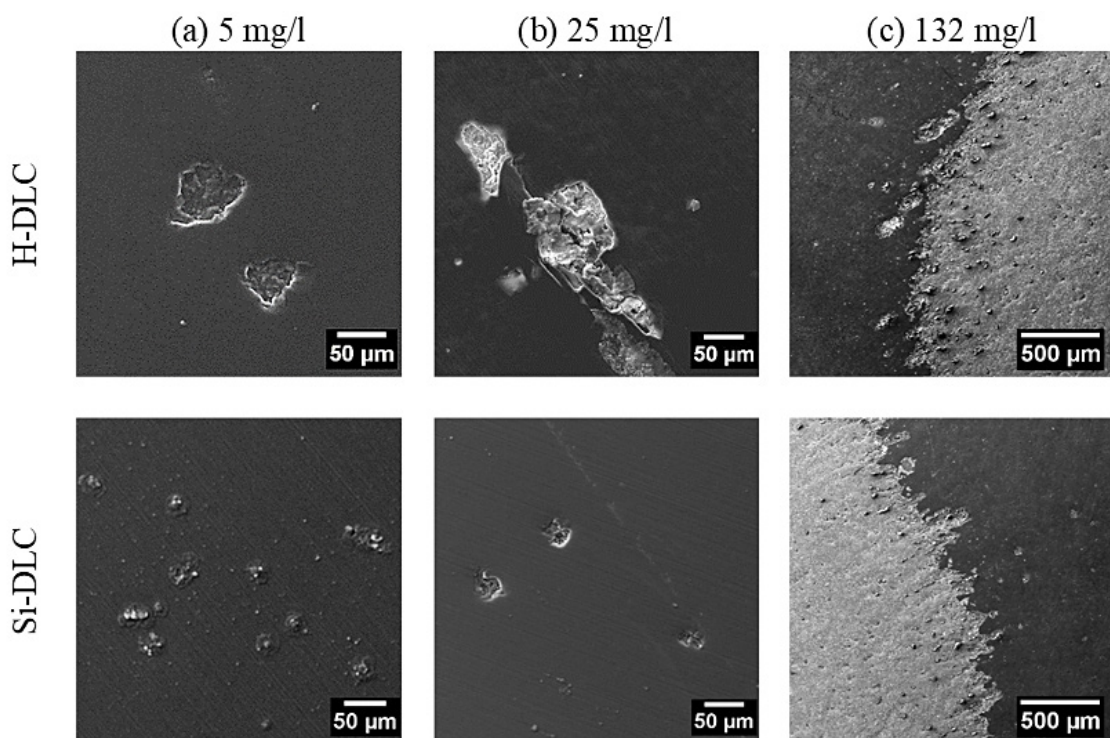
Figure 7. SEM secondary electron images of H-DLC and Si-DLC films subjected to erosion with a velocity of 10 m/s and sand concentration of (a) 5, (b) 25 and (c)132 mg/l.

load-bearing capacity diminishes due to failures in the film, resembling flakes. Figures 7a and b show the failure at the surface of the DLC films. At a velocity of 10 m/s, partial or complete coating removal occurs, depending on the sand concentration in the solution. Cheng and Jiang[7] observed detachment or delamination of DLC coatings and attributed these failures to insufficient adhesion between the coating and the metallic substrate, which compromises the coating's integrity under erosive conditions. These authors also reported the appearance of small grooves and delamination of the film, highlighting the connection between these phenomena and mechanical response of the material under erosive stress. Figure 7 suggests that a critical level of erosion was reached in the conditions of 10 m/s velocity and 5 mg/l of sand concentration, since nucleation of fatigue cracks and pits were induced on the DLC surface. According to Cheng and Jiang[7], the initiation sites of these failures are associated with locations of stress concentration in the coating such as polishing traces and small surface defects.

Erosion resistance of DLC films is associated with the elastic modulus, hardness, fracture toughness and impact angle of the sand particles[28-33]. The lower measured values of hardness and elastic modulus for the Si-DLC film, as compared to the H-DLC, suggests a higher absorption capacity for the impact caused by the impinging particles resulting in reduced initiation, propagation and coalescence of cracks in the film and a lower overall mass loss during erosion. Cheng and Jiang[7] reported similar results, where lower hardness DLC films showed reduced loss in thickness during erosion.
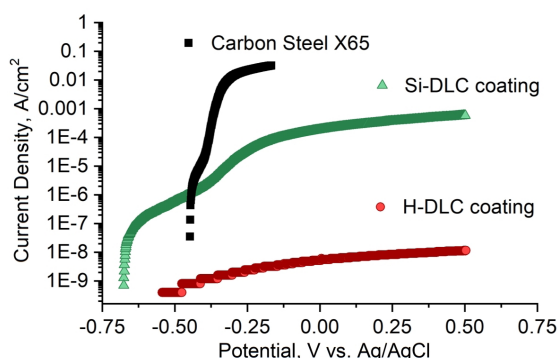

Figure 8. Anodic polarisation curves of H-DLC and Si-DLC coatings and bare steel in 3,5% NaCl, naturally aerated.

The literature presents similar results showing the improvement on the erosion and corrosion resistance of substrate covered with DLC films, especially with Si-DLC[34-37].

3.3 Electrochemical tests

The anodic polarization curves of carbon steel, as well as the H-DLC and Si-DLC coatings in naturally aerated 3.5% NaCl solution and static conditions are shown in Figure 8 followed by provided data in Table 2.

The carbon steel showed active dissolution in the solution (Figure 8). The H-DLC film and the carbon steel showed similar values of OCP: -0.543 and -0.477 mV, respectively, therefore, the galvanic couple formed between

**Table 2.** Open circuit potential (OCP), current density values measured at OCP, 100 and 200 mV above the OCP.

Sample	Solution	pH	OCP (V) (Ag/AgCl/KCl)	Pot. (V) 100mV above OCP	i (A/cm²) 100mV above OCP	Pot. (V) 200mV above OCP	i (A/cm²) 200mV above OCP
X65 Steel			-0.477	-0.377	1.70E-04	-0.277	1.77E-02
H-DLC	3.5% NaCl	7	-0.543	-0.443	8.00E-10	-0.343	1.60E-09
Si-DLC			-0.676	-0.576	2.48E-07	-0.476	7.67E-07
Condition	R_s (KΩ.cm²)	CPE_1 (F.s$^{α-1}$.cm^{-2})	$α_{CPE1}$	R_1 (KΩ.cm²)	CPE_2 (F.s$^{α-1}$.cm^{-2})	$α_{CPE1}$	R_2 (KΩ.cm²)
X65 Steel	0.421	0.204e^{-3}	0.846	6.363	---	---	---
Si-DLC	2.522	0.674^{-6}	0.534	9.484	0.6819e^{-6}	0.879	75.453
H-DLC	6.023	0.314e^{-6}	0.412	19.342	0.5292e^{-6}	0.863	126.918

them is extremely low. The results agree with literature[2,3]. Wang et al.[2] showed that a failure in a DLC film exposing the metal surface will not cause localized corrosion, due to that fact that surfaces exposed have almost the same OCP. Hadinata et al.[1] also showed that DLC coated samples, both with and without defects had similar OCPs to carbon steel; the OCP of Si-DLC films was found to be more negative then H-DLC so, more susceptible to forming a galvanic couple.

The results were evaluated based on the electrochemical equilibrium Pourbaix diagram for the Fe/H$_2$O system at 25°C[18]. Both DLC coatings showed higher corrosion resistance than the carbon steel substrate, as expected (Table 2). Carbon steel showed the highest corrosion current density (by Tafel extrapolation) by 2 orders of magnitude.

The lower anodic current density of DLC films compared to carbon steel is well known[1,14,15,18,19-22]. However, there are few reports correlating the DLC current density with the dissolution process on the DLC coating or bulk material. Two variables need to be analyzed in this context: first, the presence of pores in the DLC film could cause a small current density (however, the films are inert, amorphous and do not corrode, so this anodic current is not related with passivation[15]); secondly, the amorphous structure could reduce or discontinue electron transport over the DLC surface. Thus, the low anodic density current is associated with the flow of ions through a nano-porous surface.

Surface defects such as nano pores can allow the solution entry into the DLC film and trigger the corrosion process on the substrate. However, if the films do not present nano defects, ion flow through the film can be understood in relation to the electrochemical equilibrium Pourbaix diagram for the Fe/H$_2$O system at 25°C[18] and would involve the reaction:

$$2H_2O \rightarrow O_2 + 4H^+ + 4e^-$$
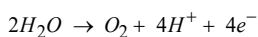
In Figure 8, the Si-DLC film has an initially low anodic current which instantly increases with the anodic potential application. Defects and anodic polarization on the surface of the film could be playing a key role in this behavior. The film deposition process potentially creates nanoscale defects which, during anodic polarization, could enable diffusion of ions[2]. Good adhesion, a high-quality coating/substrate interface and an apparently undefective deposited film were seen for the H-DLC coatings. The low anodic current

of the H-DLC (Table 2) suggests an excellent resistivity to corrosion processes in saline solutions.

EIS curves for carbon steel, H-DLC and Si-DLC films in 3.5% NaCl solution at OCP are plotted in Figure 9. Figure 9a shows the Nyquist plots at high, intermediate and low frequencies. Both DLC coatings showed higher values of Z_{real} and Z_{imag} at intermediate and low frequencies, suggesting a higher capacitance and increased corrosion resistance compared to carbon steel. The capacitive arcs of both DLC films are higher than the carbon steel, illustrating the high polarization resistance and resistivity of the films. The Si-DLC film showed a capacitive arc smaller than the H-DLC film which most likely arose from nano defects in the film, allowing saline solution penetration, causing corrosion of the metal substrate and reducing the capacitive arc. The results are in accordance with polarization findings (Figure 8), where the Si-DLC coating showed a higher anodic density current than the H-DLC coating.

At low frequencies both DLC coatings presented a higher Z modulus than carbon steel, implying excellent corrosion resistance of the coatings. The low contact time could explain the electrochemical corrosion reactions between the interface of DLC films and carbon steel substrate. Thus, ion transport could be avoided due to the DLC layer[2]. Furthermore, the decrease of Z modulus for Si-DLC can be related to surface nano defects.

Examining the Bode plots (Figure 9b), it can be observed that on going from high frequencies to low frequencies, the impedance process moves from Ohmic- to capacitance-dominating[33]. The phase shifts range from 0° to -68°, -38° and -45° for carbon steel, H-DLC and Si-DLC coatings, respectively. The presence of a single constant time or maximum angle for the carbon steel is observed, while there are two time constants or two maximum angles for both DLC films. This angle at high frequencies could be associated with the inert properties of the DLC films, which are effective as a barrier to charge transfer (electrochemical reaction) at the DLC/ electrolyte interface. The angle at intermediate frequencies angle may be related to DLC capacitance (CPE_1).

Figure 10 shows the equivalent circuits used to model the EIS results and Table 3 presents the values obtained by fitting. The DLC film equivalent circuit was fitted using: an electrolyte solution resistance (Rs); a DLC coating capacitance as a constant phase element (CPE_1); a resistance
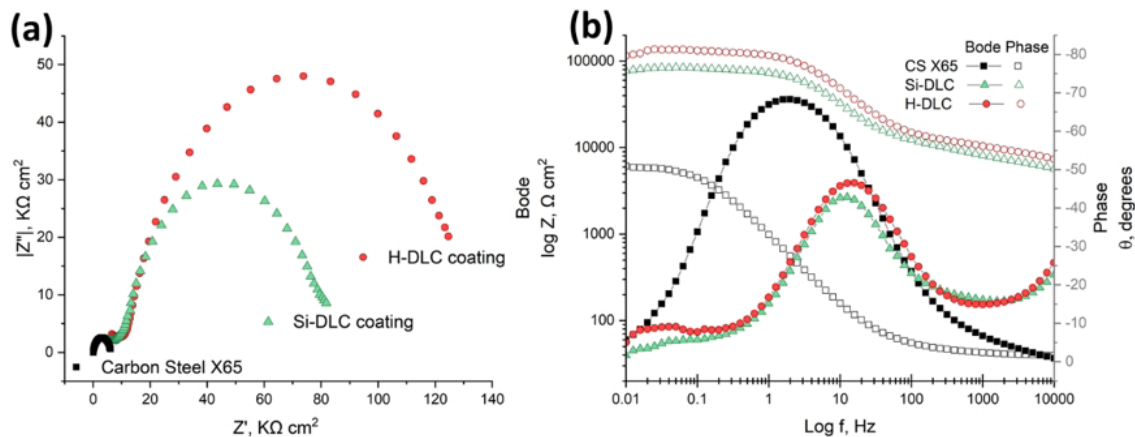
Figure 9. EIS plots for the carbon steel, H-DLC and Si-DLC films: (a) Nyquist, (b) Bode & Phase diagrams.
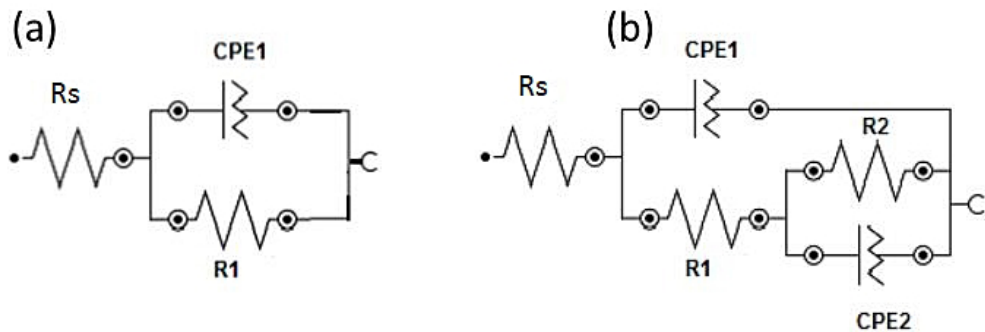

Figure 10. Equivalent circuit of: (a) the carbon steel and (b) DLC film coatings.

Table 3. Electrochemical impedance parameters fitted from the measured EIS data.

Condition	R_s ($K\Omega.cm^2$)	CPE_1 ($F.s^{\alpha-1}.cm^{-2}$)	α_{CPE1}	R_1 ($K\Omega.cm^2$)	CPE_2 ($F.s^{\alpha-1}.cm^{-2}$)	α_{CPE1}	R_2 ($K\Omega.cm^2$)
X65 Steel	0.421	$0.204e^{-3}$	0.846	6.363	---	---	---
Si-DLC	2.522	0.674^{-6}	0.534	9.484	$0.6819e^{-6}$	0.879	75.453
H-DLC	6.023	$0.314e^{-6}$	0.412	19.342	$0.5292e^{-6}$	0.863	126.918

to charge transfer at the DLC film/electrolyte interface, a DLC surface associated with areas of ionic conduction expressed as porous resistance (R_1); the polarization resistance of the charge transfer and capacitance of DLC/ substrate interface represented by the elements R_2 and CPE_2 in parallel, implying a DLC internal layer. The equivalent circuit of the carbon steel (substrate) was fitted using: an electrolyte solution resistance (Rs); a capacitance of the substrate, being a constant phase element (CPE_1) and resistance to charge transfer between the solution and the substrate (R_1), in parallel.

The impedance of the DLC films at high frequencies is controlled by the electrolyte resistance (R_e), that has a dominant Ohmic behaviour. At intermediate frequencies, the system is controlled by the capacitance of the DLC films (CPE_1) and the resistance to charge transfer at the DLC film/electrolyte interface (R_1). At low frequencies (10^{-3} to 10^{-1} Hz), the impedance is controlled by the polarisation resistance

to transfer charge between the DLC film and the substrate interface (R_2) and by the capacitance of interface (CPE_2).

4. Conclusions

The experiments analyzed the influence of flow velocity and sand concentration on the erosion and corrosion resistance of hydrogenated DLC and hydrogenated-silicon DLC coatings deposited on carbon steel. The following conclusions can be drawn:

- DLC coated carbon steels did not lose mass in low speed erosion tests and in the absence of sand. However, lower sand concentrations and speed (5 mg/l and 10 m/s) were sufficient to cause the nucleation of cracks and fatigue wells at the surface of the DLC films. The initiation sites of these defects could be associated with stress concentration sites e.g., surface coating failures. The mass loss and

micro detachment increased as the concentration of sand and the flow velocities increased.

- The Si-DLC film revealed less mass loss and lower hardness than the H-DLC film. The higher ductility of the Si-DLC makes it more prone to degrade by the erosion process. In that case, the absorption capacity of the impact strength caused by the impinging solution with sand particles was higher to Si-DLC.

- The OCP voltages of the DLC coatings had almost the same value as the carbon steel, forming very small galvanic couples between the coatings and the carbon steel substrate. Therefore, if a defect appears on the DLC coatings, the localized corrosion would be inhibited.

- The DLC films act as a corrosion barrier, a desirable property to improve corrosion resistance of carbon steels in saline solution environments. However, the anodic current increased after anodic potential applying. This increasing current probably occurred because of the process of film deposition that could possibly have created some nanoscale defects and, at high anodic potentials, the diffusion of ions inside these defects could initiate the corrosion process on metal surface.

- The lower anodic current density of the DLC films in relation to the carbon steel, around nA/cm^2 suggests a high resistivity of these films and an ionic transport mechanism under the DLC surface which is related to the process of water splitting. This could be explained by the pores presence in the DLC film.

5. Acknowledgments

6. References

1. Hadinata S-S, Lee M-T, Pan S-J, Tsai W-T, Tai C-Y, Shih C-F. Electrochemical performances of diamond-like carbon coatings on carbon steel, stainless steel, and brass. Thin Solid Films. 2013;529:412-6. http://doi.org/10.1016/j.tsf.2012.05.041.

2. Wang ZM, Zhang J, Han X, Li QF, Wang ZL, Wei R. Corrosion and salt scale resistance of multilayered diamond-like carbon film in CO2 saturated solutions. Corros Sci. 2014;86:261-7. http://doi.org/10.1016/j.corsci.2014.05.015.

3. Hu X, Neville A. CO2 erosion–corrosion of pipeline steel (API X65) in oil and gas conditions: a systematic approach. Wear. 2009;267(11):2027-32. http://doi.org/10.1016/j.wear.2009.07.023.

4. Barker R, Hu X, Neville A. The influence of high shear and sand impingement on preferential weld corrosion of carbon steel pipework in CO2-saturated environments. Tribol Int. 2013;68:17-25. http://doi.org/10.1016/j.triboint.2012.11.015.

5. Depner-Miller U, Ellermeier J, Scheerer H, Oechsner M, Bobzin K, Bagcivan N, et al. Influence of application technology on the erosion resistance of DLC coatings. Surf Coat Tech. 2013;237:284-91. http://doi.org/10.1016/j.surfcoat.2013.07.043.

6. Jellesen MS, Christiansen TL, Hilbert LR, Møller P. Erosion–corrosion and corrosion properties of DLC coated low temperature gas-nitrided austenitic stainless steel. Wear. 2009;267(9-10):1709-14. http://doi.org/10.1016/j.wear.2009.06.038.

7. Cheng F, Jiang S. Cavitation erosion resistance of diamond-like carbon coating on stainless steel. Appl Surf Sci. 2014;292:16-26. http://doi.org/10.1016/j.apsusc.2013.11.044.

8. Trakhtenberg IS, Vladimirov AB, Plotnikov SA, Rubshtein AP, Vykhodets VB, Bakunin OM. Effect of adhesion strength of DLC to steel on the coating erosion mechanism. Diam Relat Mater. 2001;10(9-10):1824-8. http://doi.org/10.1016/S0925-9635(01)00430-7.

9. Jia Z, Xia Y, Li J, Pang X, Shao X. Friction and wear behavior of diamond-like carbon coating on plasma nitrided mild steel under boundary lubrication. Tribol Int. 2010;43(1-2):474-82. http://doi.org/10.1016/j.triboint.2009.07.012.

10. Zhou ZF, Li KY, Bello I, Lee CS, Lee ST. Study of tribological performance of ECR–CVD diamond-like carbon coatings on steel substrates. Wear. 2005;258(10):1589-99. http://doi.org/10.1016/j.wear.2004.10.005.

11. Pang H, Wang X, Zhang G, Chen H, Lv G, Yang S. Characterization of diamond-like carbon films by SEM, XRD and Raman spectroscopy. Appl Surf Sci. 2010;256(21):6403-7. http://doi.org/10.1016/j.apsusc.2010.04.025.

12. American Petroleum Institute. API RP 14E: recommended practice for design and installation of offshore production platform piping systems. Washington: American Petroleum Institute; 1991.

13. Dalibon EL, Escalada L, Simison S, Forsich C, Heim D, Bruhl SP. Mechanical and corrosion behavior of thick and soft DLC coatings. Surf Coat Tech. 2017;312:101-9. http://doi.org/10.1016/j.surfcoat.2016.10.006.

14. Liu E, Kwek HW. Electrochemical performance of diamond-like carbon thin films. Thin Solid Films. 2008;516(16):5201-5. http://doi.org/10.1016/j.tsf.2007.07.089.

15. Reisel G, Irmer G, Wielage B, Dorner-Reisel A. Electrochemical corrosion behavior of carbon-based thin films in chloride ions containing electrolytes. Thin Solid Films. 2006;515(3):1038-42. http://doi.org/10.1016/j.tsf.2006.07.063.

16. Veres M, Koós M, Tóth S, Füle M, Pócsik I, Tóth A, et al. Characterisation of a-C:H and oxygen-containing Si:C:H films by Raman spectroscopy and XPS. Diam Relat Mater. 2005;14(3-7):1051-6. http://doi.org/10.1016/j.diamond.2005.01.020.

17. Papakonstantinou P, Zhao J, Lemoine P, McAdams ET, McLaughlin JA. The effects of Si incorporation on the electrochemical and nanomechanical properties of DLC thin films. Diam Relat Mater. 2002;11(3-6):1074-80. http://doi.org/10.1016/S0925-9635(01)00656-2.

18. Pourbaix M, Burbank J. Atlas D-Equilbres electrochimiques. J Electrochem Soc. 1964;111(1):14C. http://doi.org/10.1149/1.2426051.

19. Sharma R, Barhai PK, Kumari N. Corrosion resistant behaviour of DLC films. Thin Solid Films. 2008;516(16):5397-403. http://doi.org/10.1016/j.tsf.2007.07.099.

20. Manhabosco TM, Barboza APM, Batista RJC, Neves BRA, Müller IL. Corrosion, wear and wear–corrosion behavior of graphite-like a-C:H films deposited on bare and nitrided titanium alloy. Diam Relat Mater. 2013;31:58-64. http://doi.org/10.1016/j.diamond.2012.11.005.

21. Robertson J. Diamond-like amorphous carbon. Mater Sci Eng R Reports. 2002;37(4-6):129-281. http://doi.org/10.1016/S0927-796X(02)00005-0.

22. Manhabosco TM, Müller IL. Tribocorrosion of diamond-like carbon deposited on Ti6Al4V. Tribol Lett. 2009;34(3):229-229. http://doi.org/10.1007/s11249-009-9417-7.

23. Solis J, Zhao H, Wang C, Verduzco JA, Bueno AS, Neville A. Tribological performance of an H-DLC coating prepared by PECVD. Appl Surf Sci. 2016;383:222-32. http://doi.org/10.1016/j.apsusc.2016.04.184.

24. Holmberg K, Matthews A. Coatings tribology: properties, mechanisms, techniques and applications in surface engineering. USA: Elsevier Science; 2009.

25. Hutchings IM. Ductile-brittle transitions and wear maps for the erosion and abrasion of brittle materials. J Phys D Appl

Phys. 1992;25(1A):A212-21. http://doi.org/10.1088/0022-3727/25/1A/033.

26. Kalin M, Vižintin J. A comparison of the tribological behaviour of steel/steel, steel/DLC and DLC/DLC contacts when lubricated with mineral and biodegradable oils. Wear. 2006;261(1):22-31. http://doi.org/10.1016/j.wear.2005.09.006.

27. Strondl C, Carvalho NM, De Hosson JTM, Krug TG. Influence of energetic ion bombardment on W-C:H coatings deposited with W and WC targets. Surf Coat Tech. 2005;200(1-4):1142-6. http://doi.org/10.1016/j.surfcoat.2005.02.182.

28. Bernoulli D, Rico A, Wyss A, Thorwarth K, Best JP, Hauert R, et al. Improved contact damage resistance of hydrogenated diamond-like carbon (DLC) with a ductile α-Ta interlayer. Diam Relat Mater. 2015;58:78-83. http://doi.org/10.1016/j.diamond.2015.06.006.

29. Pandey B, Pal PP, Bera S, Ray SK, Kar AK. Effect of nickel incorporation on microstructural and optical properties of electrodeposited diamond like carbon (DLC) thin films. Appl Surf Sci. 2012;261:789-99. http://doi.org/10.1016/j.apsusc.2012.08.101.

30. Constantinou M, Pervolaraki M, Nikolaou P, Prouskas C, Patsalas P, Kelires P, et al. Microstructure and nanomechanical properties of pulsed excimer laser deposited DLC:Ag films: Enhanced nanotribological response. Surf Coat Tech. 2017;309:320-30. http://doi.org/10.1016/j.surfcoat.2016.11.084.

31. Souza RC, Santos BAF, Gonçalves MC, Mendes EP Jr, Simões TA, Oliveira JR, et al. The role of temperature and H2S (thiosulfate) on the corrosion products of API X65 carbon steel exposed to sweet environment. J Pet Sci Eng. 2019.

32. Dhandapani VS, Kang K-M, Seo K-J, Kim C-L, Kim D-E. Enhancement of tribological properties of DLC by incorporation of amorphous titanium using magnetron sputtering process. Ceram Int. 2019;45(9):11971-81. http://doi.org/10.1016/j.ceramint.2019.03.090.

33. Souza RC, Santos BAF, Gonçalves MC, Mendes EP Jr, Simões TA, Oliveira JR, et al. The role of temperature and H2S (thiosulfate) on the corrosion products of API X65 carbon steel exposed to sweet environment. J Pet Sci Eng. 2019;180:78-88. http://doi.org/10.1016/j.petrol.2019.05.036.

34. Zur I, Shmanay Y, Fedotova J, Remnev G, Movchan S, Uglov V. Erosion mechanisms of DLC coatings deposited on polyimide and silica substrates when exposed to a pulsed gas discharge. Diam Relat Mater. 2024;142:110802. http://doi.org/10.1016/j.diamond.2024.110802.

35. Jellesen MS, Christiansen T, Hilbert LR, Møller P. Erosion–corrosion and corrosion properties of DLC coated low temperature gas-nitrided austenitic stainless steel. Wear. 2009;267(9-10):1709-14. http://doi.org/10.1016/j.wear.2009.06.038.

36. Xu LI, Haodong WU, Jiaying JIN, Dongxu CHEN, Hongyun DENG, Yanwen ZHOU. Erosion corrosion behavior of Si-DLC film deposited on 2024 aluminum alloy. Chin J Vac Sci Technol. 2023;43(2):134-41. http://doi.org/10.13922/j.cnki.cjvst.202206020.

37. Sam SJM, Liskiewicz TW, Neville A, Beake BD. Probing fatigue resistance in multi-layer DLC coatings by micro- and nano-impact: correlation to erosion tests. Surf Coat Tech. 2020;402:126319. http://doi.org/10.1016/j.surfcoat.2020.126319.